AIAA 82-4010

Floating Shock Fitting for Three-Dimensional Inviscid Supersonic Flows

Y. Yamamoto*
National Aerospace Laboratory, Tokyo, Japan
and
K. Karashima†
Institute of Space and Astronautical Science, Tokyo, Japan

A numerical approach based on marching procedures is presented for three-dimensional supersonic flows involving shock-shock interactions, where the shock waves and the associated contact surfaces are determined as floating discontinuities in a fixed system of computational meshes. In order to calculate the regions having subsonic velocity components in the marching direction, which are embedded locally in a supersonic flowfield, a numerical method is also developed that is easily adaptable to the conventional marching procedures. The method consists of an alternate iteration of time-dependent and marching schemes, in which an explicit finite-difference algorithm is employed to solve Euler's nonconservative equations. The results of complicated three-dimensional flowfields about typical blunt-nosed wing/body combinations at angles of attack are presented to demonstrate the validity as well as the applicability of the present approach.

Introduction

IN the design of supersonic/hypersonic flight vehicles such as the Space Shuttle and other re-entry bodies, detailed knowledge of the structure of the associated three-dimensional flowfield is of paramount importance in order to estimate the aerodynamic loads and heating characteristics of the vehicles. In such an intricate three-dimensional flowfield, there exist various shock waves, expansion waves, and contact surfaces resulting from mutual interactions of these discontinuities.

A number of numerical studies developed for inviscid supersonic flows may be classified into three categories. One is based on the method of characteristics, which has been applied successfully to primarily two-dimensional flows. This method was extended by Rakich[1] and Chu[2] to the flows past wing/body combinations, although the embedded shock waves were not included in their flows. Another is the shock-capturing finite-difference method,[3-5] in which shock waves are resolved automatically by the inherent properties of conservative difference scheme and internal dissipation. However, the capability of capturing the internal shock waves by this method seems to depend largely upon the shock strength. For instance, it is pointed out that the increase in the strength of the crossflow shock wave is apt to induce an unstable pressure oscillation near the captured preshock wave which, in turn, results in a negative pressure, thus causing the calculation to stop. The third category is known as the shock-fitting method, in which the embedded shock waves are treated explicitly as an internal boundary existing in the entire computational domain. This method has been successfully applied to the calculation of the wing/body flowfield by Moretti[6,7] and Marconi et al.[8] However, a topological difficulty arises in this method due to appearance of nonrectangular regions if shock-shock interactions occur.

In order to overcome the difficulty mentioned above, an alternative finite-difference method has been developed. Moretti[9] called his technique "floating shock fitting" to distinguish it from other sharp-shock schemes. In this procedure the shock waves propagate in the computational domain as discontinuous surfaces. The finite-difference meshes are held fixed to compute the smooth flow regions and they are not used to follow the shock waves. The topological problems associated with fitting shocks as boundaries are thereby avoided. Although the floating shock-fitting technique has been applied to calculate a complicated two-dimensional flow[10] involving many embedded shock-shock interactions, it has not yet been developed successfully for three-dimensional cases except for a conical flow problem.[11]

In the case of three-dimensional, steady, inviscid supersonic flows past aerodynamic bodies, calculations can be made numerically using the so-called marching procedures. In all such schemes the marching is generally directed along the body axis and the data at a station (i.e., the plane normal to the marching direction) are used to compute the flowfield at the next station downstream. The only inherent limitation in this method is that the velocity component in the marching direction must be supersonic everywhere in the flowfield.

However, a region of subsonic axial Mach number will sometimes be encountered near the canopy and leading edge of the wings, though the resultant flow may still remain supersonic. In such regions the same marching procedure that has been utilized in the supersonic region upstream is no longer applicable and, consequently, the calculation stops. It must be noted that the region of the subsonic axial Mach number locally occupies only a small domain embedded in the supersonic flowfield, because the flow is accelerated fairly abruptly to recover the supersonic axial Mach number again.

The fact that the resultant Mach number remains supersonic implies that the physical nature of the flow makes the marching procedure legitimate; the failure is merely in the choice of the basic frame of reference associated with the marching direction. A scheme which uses a local frame of reference has recently been developed by Marconi.[12,13] However, this method requires a cumbersome procedure and is not applicable to the flows with pockets of subsonic total Mach numbers.

It is the purpose of this study to extend the floating shock-fitting technique to three-dimensional flows involving shock-shock interactions and to present an efficient method for calculating the region of locally embedded subsonic axial Mach numbers in order to magnify the applicability of the marching procedure. This method consists of an alternate

Received Dec. 22, 1980; revision received May 27, 1981.

*Research Scientist, First Aerodynamics Division. Member AIAA.

†Professor, Research Division for Space Transportation.

iteration of time-dependent and marching procedures and is easily adaptable to the conventional marching procedures used to calculate the surrounding supersonic flowfield. Moreover, the method has an advantage of computing not only the flows with pockets of subsonic axial Mach numbers but also the flows with pockets of subsonic total Mach numbers.

Computational Frame

Take a cylindrical coordinate system (r, θ, z) such as illustrated in Fig. 1. Since the flow variables vary rapidly in the cross-sectional plane, a transformation of the independent variables is introduced to cluster the mesh points in the region of suspected large gradients. Conformal mappings, which were proposed by Moretti[7] and have been successfully applied by Marconi,[8] are introduced such as

$$\begin{aligned} \zeta &= R \cdot e^{i\Theta} \\ WW &= \zeta - F^2/4\zeta \\ W &= WW + i \cdot E \\ GG &= W + D^2/4W \\ G &= GG + i \cdot C \\ G &= r \cdot e^{i\theta} \\ Z &= z \end{aligned} \tag{1}$$

where G and ζ are the complex coordinates in the physical and mapped planes, respectively. All of the real coefficients C, D, E, and F are continuous functions of the axial coordinate z (given in Ref. 14). In these mappings the body cross section is transformed into a near circle in the mapped plane. Finally, as is introduced conventionally in the problems of this type, the distance between the body and bow shock waves is normalized into a rectangular region (computational plane) by letting

$$\begin{aligned} X &= [R - R_b(\Theta,Z)]/[R_s(\Theta,Z) - R_b(\Theta,Z)] \\ Y &= \Theta \\ Z &= Z \end{aligned} \tag{2}$$

where R and Θ are the radial and circumferential coordinates in the mapped plane, respectively. Subscripts s and b denote conditions at the shock wave and body surface, respectively.

Using the series of transformations mentioned above, the mesh points, which are evenly spaced in the computational plane, are clustered near the wing leading edge in the physical plane, so that the calculation can be carried out successfully in the region of large curvature. This circumstance is demonstrated in Fig. 2.

In computing the region of the subsonic axial Mach number, time τ is added as an independent variable to the shock shape equations in Eq. (2).

$$\begin{aligned} X &= [R - R_b(\Theta,Z)]/[R_s(t,\Theta,Z) - R_b(\Theta,Z)] \\ Y &= \Theta, \quad Z = Z, \quad \tau = t \end{aligned} \tag{3}$$

Basic Equations

The steady and unsteady three-dimensional Euler equations in cylindrical coordinates (Fig. 1) are used in the nonconservative form. With the transformation of the independent variables from physical to computational planes, the basic equations may be written in the form as

$$f_Z + [A_1]f_X + [A_2]f_Y + A_3 = 0 \tag{4}$$

$$f_\tau + [B_1]f_Z + [B_2]f_X + [B_3]f_Y + B_4 = 0 \tag{5}$$

where f denotes a row vector with $f = (P, u, v, w, \rho)$, (u, v, w) velocity components, P pressure, and ρ density. These flow quantities have been normalized by use of the freestream values such as U_∞, $\rho_\infty U_\infty^2$, and ρ_∞, respectively, where U_∞ is the freestream velocity. $[A_1]$, $[A_2]$ and $[B_1]$, $[B_2]$, $[B_3]$ are the coefficient matrices and A_3, B_4 are row vectors.

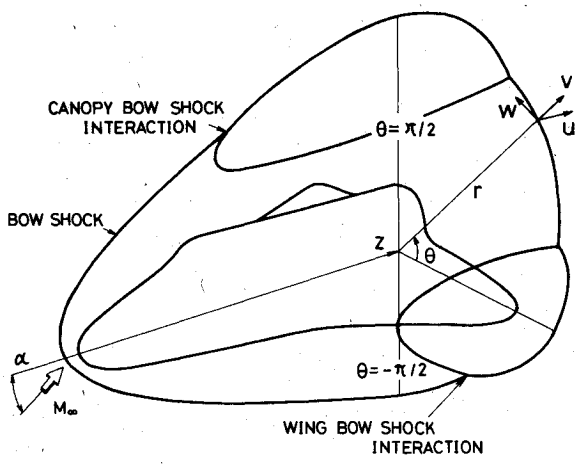

Fig. 1 Coordinate system.

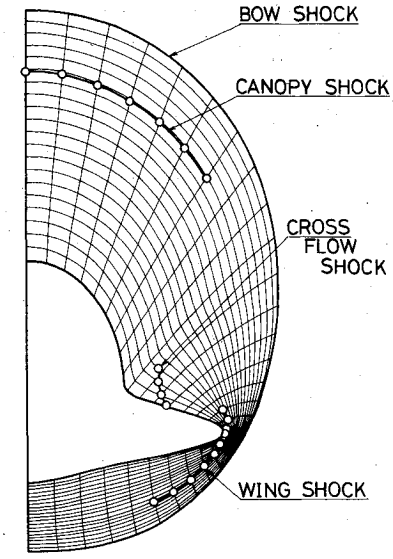

a)

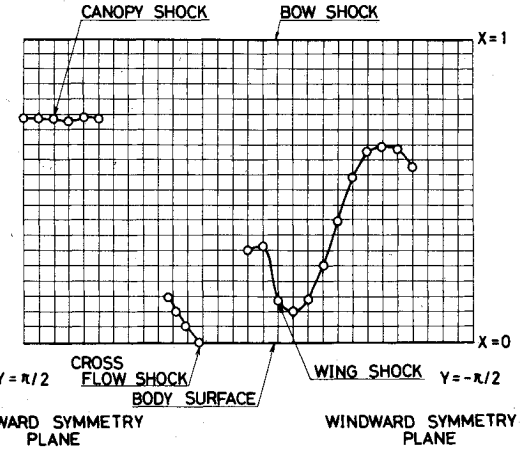

b)

Fig. 2 Mesh distribution and floating discontinuities in the physical and computational plane.

If the axial velocity component u is supersonic everywhere, the governing equation (4) is hyperbolic with respect to the body axis Z. Therefore, Eq. (4) can be integrated numerically step by step in the Z direction starting with the given initial conditions, where MacCormack's second-order, noncentered, predictor-corrector algorithm[15] is used to advance the marching step. On the other hand, the governing equation (5) is hyperbolic with respect to time τ so that it can be integrated numerically step by step in the τ direction, where MacCormack's algorithm is also applied to advance the flowfield. The step size ΔZ and $\Delta\tau$ are so determined as to satisfy the *C-F-L* condition for stability.

Special Discretization Formulas

In the floating shock-fitting approach the calculation domain is taken as single region as illustrated in Fig. 2b, where the mesh points are equally spaced and all discontinuities are allowed to move or float freely beyond the fixed grid. In this technique, it is not permitted to make finite-difference approximations by taking the mesh points that exist on the opposite sides of the discontinuity. Appropriate approximations formulated to maintain stability and accuracy of the computation must be introduced to replace this difference. These finite-difference approximations and procedures of the floating shock-fitting technique have been detailed in Refs. 9-11 and 14.

Boundary Conditions for Marching Procedure

In the present approach the Thomas scheme[16] is used for calculating the bow shock propagation. The embedded shock waves are computed by an appropriate characteristic method, where Rankine-Hugoniot conditions are applied to the discontinuities. In these calculations, the flow variables upstream of the embedded shock waves must be integrated along the shock surface. For this purpose, it will be convenient to introduce a discontinuity-oriented coordinates system, which may be expressed for the wing-type shock waves in the form

$$X=[R-R_b(\Theta,Z)]/[R_w(\Theta,Z)-R_b(\Theta,Z)]$$

$$Y=\Theta, \qquad Z=z \tag{6}$$

where $R_w(\Theta,Z)$ denotes the wing-type shock contour in the mapped plane.

The characteristic equations in the X-Z plane, which are derived from the momentum and energy equations, may be expressed as

$$\lambda_\pm=(uA-a^2X_z\pm a\beta)/(u^2-a^2) \tag{7}$$

$$\mp a\beta(P_Z+\lambda_\pm P_X)+\gamma PB(u_Z+\lambda_\pm u_X)-\gamma PuX_r(v_Z+\lambda_\pm v_X)$$

$$-\gamma PuY_\theta(w_Z+\lambda_\pm w_X)/r=l_1R_1+l_2R_2+l_3R_3+l_4R_4 \tag{8}$$

where Eqs. (7) and (8) denote characteristic directions and compatibility relations, respectively, and where

$$l_1=A-\lambda_\pm u, \quad l_2=-\gamma P(X_z-\lambda_\pm)$$

$$l_3=-\gamma PX_r, \quad l_4=-\gamma PX_\theta/r$$

$$\beta=\sqrt{(u^2-a^2)(X_r^2+X_\theta^2/r^2)+B^2}$$

$$A=uX_z+B, \quad B=vX_r+wX_\theta/r$$

$$R_1=-[HP_Y+eP(Y_zu_Y+Y_rv_Y+Y_\theta w_Y/r+v/r)] \tag{9}$$

$$R_2=-[Hu_Y+Y_zP_Y/\rho]$$

$$R_3=-[Hv_Y-w^2/r+Y_rP_Y/k]$$

$$R_4=-[Hw_Y+vw/r+Y_\theta P_Y/kr]$$

$$H=uY_z+vY_r+wY_\theta/r$$

where a is the speed of sound. It must be noted that only the up-running characteristic equations are employed for shock calculations. The application of Eq. (8) with simultaneous use of the shock relations requires an iterative procedure for determining the shock inclination $R_{w_Z}(\Theta,Z)$.

Since the crossflow shock waves are traced along the $Y=$const lines, the associated transformation of the coordinates into those aligned with the discontinuity may be expressed as

$$\bar{X}=X$$

$$\bar{Y}=(\pi/2-Y)/Y_s(X,Z) \tag{10}$$

$$\bar{Z}=Z$$

where the crossflow shock is given by $Y=Y_s(X, Z)$ in the computational plane. The characteristic equations in the Y-Z plane are similar to those for the wing-type shock waves. The tangency condition that must be satisfied by the crossflow shock points at the body surface requires that the shock waves be normal to the surface. The subsequent procedure for determining the shock-wave inclination is the same as that for the wing-type shock waves.

The boundary conditions at the body surface can be treated in the same way as Kentzer's impermeable wall scheme.[17] In Kentzer's approach, the tangency condition at the surface is differentiated and connected with the compatibility relation along the down-running characteristics in the X-Z plane, resulting in a differential equation for the surface pressure such as

$$P_Z=-\lambda_-P_X+\{\gamma Pu\tilde{R}+\gamma Pu\lambda_-[A_X-u(X_{zb})_X-v(X_{rb})_X$$

$$-w(X_{\theta b}/r)_X]+R\}/a\beta \tag{11}$$

$$\tilde{R}=-u(X_{zb})_Z-v(X_{rb})_Z-w(X_{\theta b})_Z/r+wr_ZX_{\theta b}/r^2$$

$$R=l_1R_1+l_2R_2+l_3R_3+l_4R_4$$

where each expression of the derivatives $(X_{zb})_Z$, $(X_{rb})_Z$, $(X_{\theta b})_Z$ and flow variables on the body surface can be derived in the same way as explained in Refs. 8 and 14.

Shock-Shock Interactions

Treatment of Shock Interactions

Since, in general, the crossflow shock waves hardly grow enough to approach other shock waves, the intersection of either wing shock wave or canopy shock wave with the bow shock wave seems to be the main feature of shock-shock interactions in the flowfield under consideration. The wing shock wave is usually first detected near the root of the wing and moves toward the bow shock wave as the calculation proceeds downstream. Therefore, if the wing shock approaches the bow shock wave within one radial mesh, a shock-shock interaction is assumed to take place there, and the resultant shock wave and the contact surface are calculated. This type of interaction is named as type VI by Edney[18] and can often be observed in the supersonic flowfield about the wing/body combinations with moderately swept leading-edge wings.[19]

Figure 3 shows a sketch of the flow pattern associated with an interaction of the two incident shock waves. In the present interaction calculation, the exact Rankine-Hugoniot relations are applied to calculate the flow conditions just aft of the shock waves, whereas the associated expansion waves required to match pressure and flow direction on both sides of

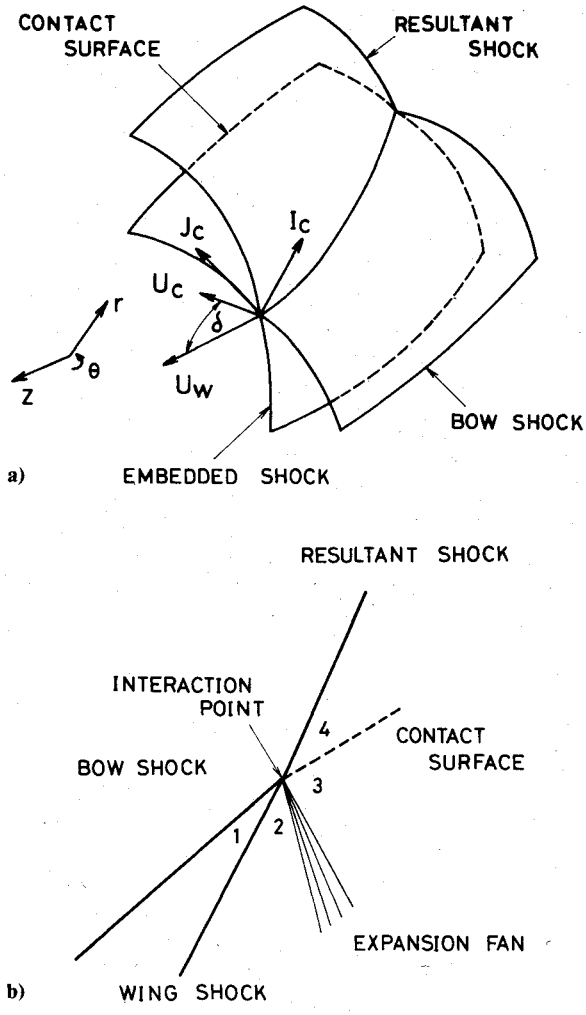

Fig. 3 Interaction scheme at the shock intersection.

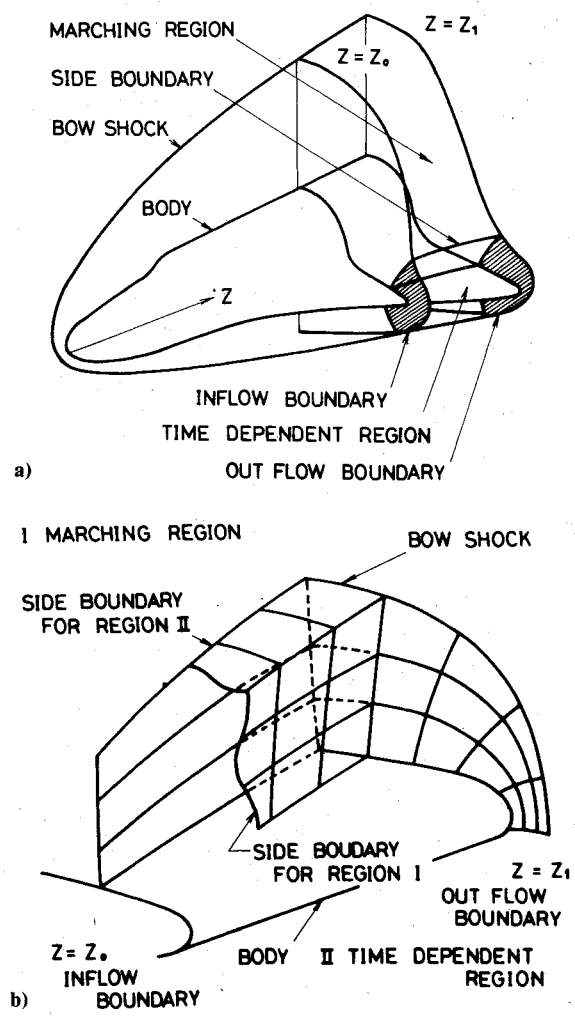

Fig. 4 Boundaries of the three-dimensional embedded region with subsonic axial Mach number.

the contact surface are evaluated approximately with an assumption that the flow crossing the expansion waves is two-dimensional in the plane made by the two unit vectors normal to the contact surface and in the Z direction, respectively (see Fig. 3a). This assumption is analogous to that proposed by Hunt.[20] Since the strength of the incident shock wave is known, the resultant shock wave and the contact surface can be determined by use of the conventional method, which may be summarized as follows.

The slope of the resultant shock wave is first assumed and Rankine-Hugoniot conditions are applied to calculate pressure and flow angle δ in region 4. The static pressure is continuous across the contact surface, and the total pressure in region 3 is equal to that of region 2 because the total pressure is kept constant through an expansion fan. With the static and total pressure, the Mach number in region 3 can be computed and the flow angle δ_e in this region is obtained through the Prandtl-Meyer relation. The procedure is iterated by adjusting the assumed slope of the resultant shock wave until the flow direction in region 3 matches that in region 4. The interaction of the canopy shock with the bow shock wave can be calculated in the same way.

The contact surface resulting from a shock-shock interaction is calculated as a discontinuous surface floating in the computational plane. Flow variables on the contact surface can be obtained in the same way as presented in Ref. 8.

Entropy Layers

In calculation of flows about blunt-nosed smooth bodies, it is well known that the entropy gradient normal to the body surface becomes increasingly steep as the calculation proceeds downstream; that is, the so-called entropy discontinuity occurs. In practical calculations, the entropy layer cannot be fully resolved numerically because the thickness of the layer will ultimately become smaller than the size of a radial mesh, even if it is made as small as possible. Because of this, in the present calculations an expedient approach is employed where the wall entropy is assumed to be given by a linear extrapolation from the interior points. This extrapolation is initiated at the shoulder of the blunted cone cylinder. As is pointed out in Ref. 5, the approximate evaluation of the wall entropy may, to a certain extent, modify the surface flow variables, except for the pressure that is the major interest in this kind of study. This approximation gradually reduces the wall entropy to eliminate ultimately the numerical discontinuities at the wall, thus resulting in magnifying the range of applicability of the numerical calculations.

A Method for Solving Subsonic Axial Mach Number Region

In general, as the swept angle of the wing leading edge becomes smaller, an embedded region of subsonic axial Mach number will arise, for which the marching procedure is no longer applicable. In this section an efficient method for calculating the subsonic axial Mach number region is presented, which is a successive procedure consisting of an alternate use of the three-dimensional time-dependent and marching schemes.

Numerical Algorithm

Figure 4a shows a sketch of the embedded region of subsonic axial velocity near the wing leading edge, for which the

time-dependent method is applied to obtain a local solution. The entire solution is determined by matching the time-dependent solution with the marching solution for the surrounding region of supersonic axial velocity using an alternate scheme. For this purpose it is necessary to set two side boundaries in the region where the axial velocity is assured to be supersonic. In Fig. 4b the upper half of the embedded region is presented. As shown in the figure, the outer side boundary is considered a temporary boundary for the time-dependent region (region II) on which the boundary values are prescribed by the marching solutions, whereas the inner side boundary is taken as a temporary boundary for the marching region (region I) on which the boundary values are given by the roughly converged time-dependent solutions. In each step of the iteration the boundary values are replaced by the new solutions obtained alternately for either the marching or the time-dependent region.

The numerical algorithm for calculating the embedded region of subsonic axial Mach number is as follows. The boundary values on the outer side boundary (i.e., values on the side boundary for region II) are first assumed and the integration of the unsteady Euler equations is executed to advance the subsonic flowfields in the time asymptotic relaxation process. After the time-dependent solution converges roughly, all internal flow values except those on the outer side boundary are fixed. Then, using the boundary values on the inner side boundary (i.e., values on the side boundary for region I), the flowfields in the marching region are determined. If the marching step size ΔZ differs from the grid size ΔZ of the subsonic region, the values on the side boundary used in a marching step are obtained by interpolation. The boundary values for the time-dependent region are then replaced by the marching solutions and the same procedure is repeated until the time-dependent solution converges to the steady state. The convergence criterion is given by the relation $(P^{n+1}-P^n)/P^n<0.005$, where n denotes the time step.

Initial and Boundary Conditions

Initial conditions for the time-dependent calculation of the subsonic embedded region are given by the marching solutions obtained previously with nearly the same conditions. The embedded subsonic region is surrounded by six boundaries, i.e., two side boundaries, the body, the bow shock wave, and the inflow ($Z=Z_0$) and the outflow ($Z=Z_1$) boundaries. The treatments of side boundaries have been described in the previous section. In the plane $Z=Z_0$ (inflow boundary), the flow variables are fixed at the values determined from the marching code. In the plane $Z=Z_1$ (outflow boundary), the flow variables are evaluated by integrating the

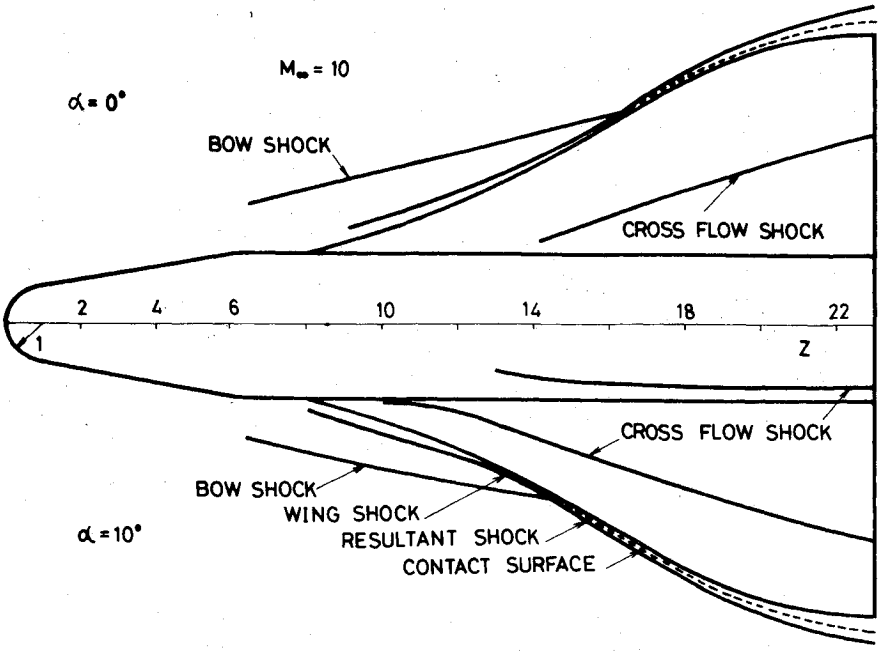

Fig. 5 Plane view for shock patterns and interactions.

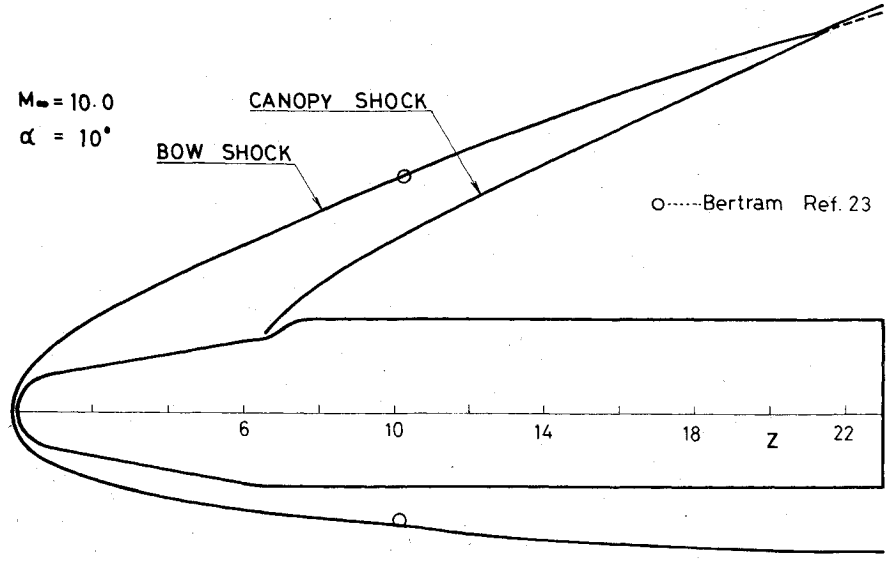

Fig. 6 Side view for shock patterns and interactions.

basic equations using backward differences in the Z direction, because the axial velocity component is supersonic everywhere. Boundary conditions at the bow shock wave and the body surface are as follows.

A modification of the pressure approach originally developed by Thomas et al.[16] for steady flow is employed to calculate the bow shock wave. The boundary conditions at the body surface can be evaluated by use of characteristic relations. Differentiation of the tangency condition at the surface with respect to time and connecting it with the three-dimensional compatibility equations obtained in the same way as proposed by Barnwell[21] then leads to the following equations for the surface pressure

$$P_\tau = -[(u-an_{bz})X_z + (v-an_{br})X_r + (w-an_{b\theta})X_\theta/r]P_X$$
$$-[(u-an_{bz})Y_z + (v-an_{br})Y_r + (w-an_{b\theta})Y_\theta/r]P_Y$$
$$-(u-an_{bz})P_Z + \rho aB(u_Y n_{bz} + v_Y n_{br} + w_Y n_{b\theta})$$
$$+\rho au(u_Z n_{bz} + v_Z n_{br} + w_Z n_{b\theta}) - \rho a^2[(u_X X_z + v_X X_r$$
$$+w_X X_\theta/r) + (u_Y Y_z + v_Y Y_r + w_Y Y_\theta/r) + u_Z] + \tilde{R} \qquad (12)$$
$$B = uY_z + vY_r + wY_\theta/r$$
$$\tilde{R} = -\rho a(w^2 n_{br} - vwn_{b\theta} + av)/r$$

where n_{br}, $n_{b\theta}$, and n_{bz} denote, rspectively, the components in the r, θ, and z directions of a unit vector normal to the body surface. Using entropy function $S(P/\rho^\gamma)$ and velocity components (v,w) obtained by integrating the r and θ momentum equations, respectively, the other flow variables at the body surface can be evaluated in a way similar to that presented in Refs. 8 and 14.

Results and Discussion

Numerical computations were carried out to demonstrate the applicability and limitation of the present approach for solving three-dimensional flowfields about wing/body combinations and the results were obtained, assuming a perfect gas, at Mach number of 10.0 and at angles of attack of 0 and 10 deg. These conditions are of a computational interest because of the various strong embedded shock waves caused by the complicated body configuration for which the fitting procedure will be more adequate than the capturing method.

In the present calculation, a spherically blunted cone-cylinder is used as the nose of a wing/body combination in the subsequent computational example. The subsonic flowfield is computed by the inverse method.[22] In the latter region, the solution is given by the general marching method without mappings.

With the solution at the shoulder of the spherically blunted cone-cylinder as the initial data, the flows past wing/body combinations were further calculated. A typical cross section of the body at a given longitudinal coordinate Z consists of a top ellipse and bottom circular body upon which is superimposed a curve generated by trigonometric functions as the wings. The wing thickness at the root remains constant, while its span grows smoothly with Z. Also the semimajor axes of the top ellipse change smoothly to simulate the canopy contour.

Numerical results obtained only by marching procedure are presented in Figs. 5-8. The shock-wave location in both planform and side views are shown in Figs. 5 and 6. In Fig. 5 the upper half of the planform corresponds to $\alpha = 0$ deg and the lower half to $\alpha = 10$ deg. In the case of $\alpha = 10$ deg, both the wing shock wave and the crossflow shock wave on the wing surface locate further upstream than in the case $\alpha = 0$ deg. Moreover, on the leeward side of the body the second crossflow shock wave appears. The same is true for the location of interactions between bow and wing shock waves.

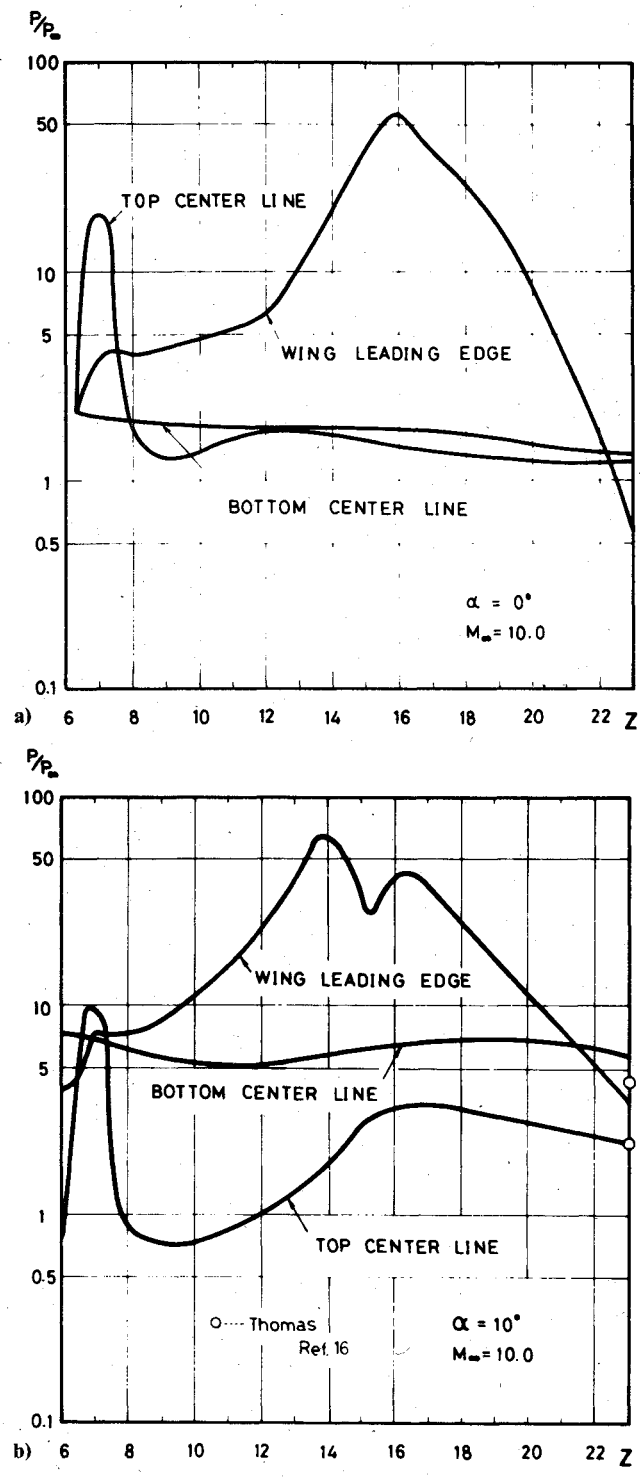

Fig. 7 Longitudinal surface pressure distribution.

The contact surface resulting from a shock-shock interaction of the same family is shown as a dashed line in the figure. In the above numerical case, the minimum swept angle of the wing leading edge which appears at $Z = 16$-17 is 60 deg.

The shock-wave shape in the side view is given in Fig. 6, where an interaction of the canopy shock with the bow wave can be seen. Since there are no existing data to be directly compared with the present results, the experimental shock-wave locations for a spherically blunted 70 deg swept delta body with elliptic cross section proposed by Betram[23] at $M_\infty = 9.6$ are also plotted in the same figure. Although they may not be suitably comparable data, the agreement between the present results and the experiment is found to be fairly good.

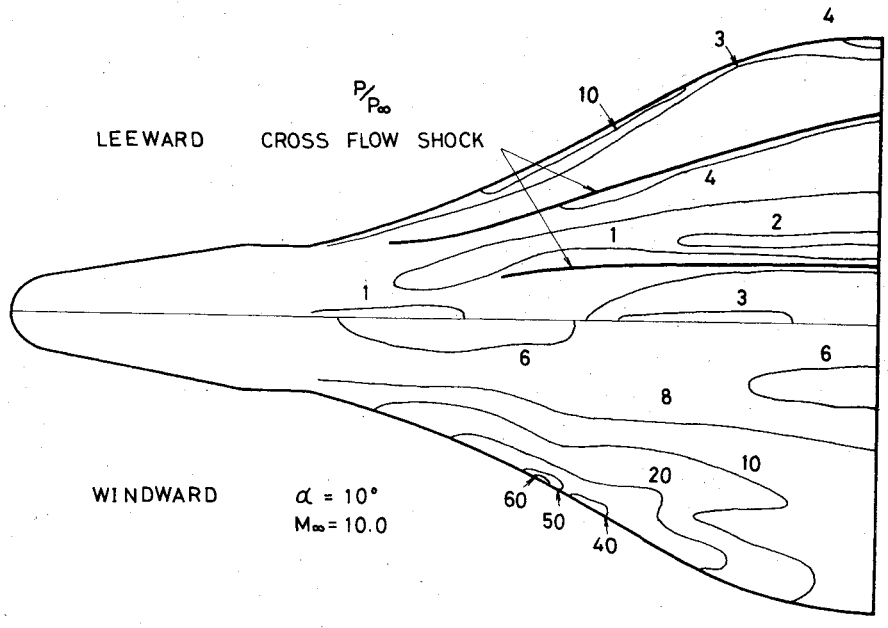

Fig. 8 Pressure contours (P/P_∞) on the body surface.

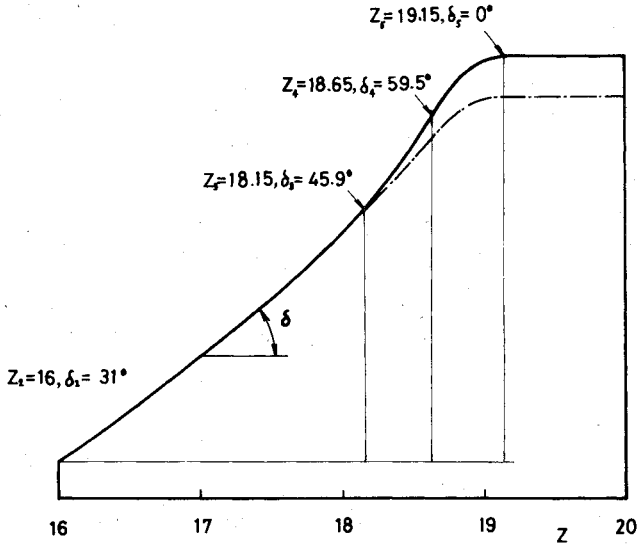

Fig. 9 Planform of the wing with subsonic axial Mach number.

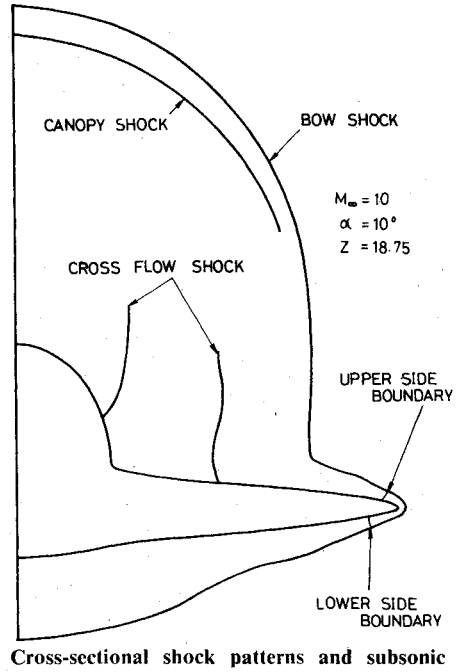

Fig. 10 Cross-sectional shock patterns and subsonic embedded region.

In Fig. 7 are shown the longitudinal surface pressure distributions in the leeward and windward planes of symmetry and the pressure distribution along the leading edge of the wing. In the leeward plane of symmetry, a rapid increase and decrease in pressure near $Z=7.0$ is clearly owing to the canopy. To adjust the overexpansion of the flow along the canopy, a weak recompression occurs downstream. The pressure rise due to the canopy becomes more conspicuous at $\alpha=10$ deg and the same trend can be seen in the results of Ref. 4. With the increase of the angle of attack, the pressure rise for adjusting the overexpansion seems to grow into a shock wave. The pressure behavior in the windward plane of symmetry is quite moderate.

The high pressure along the leading edge is obviously due to a strong recompression through the wing shock wave. Its qualitative behavior seems to depend nearly on the local angle of the swept leading edge, because the present wing has the minimum swept angle of 60 deg at $Z=16$-17 and the increase in pressure corresponds roughly to the decrease in local swept angle, except in the vicinity of the point of shock interaction. However, it must be remarked in the case of $\alpha=10$ deg that a local minimum in leading-edge pressure occurs slightly downstream of the point of interaction. In this case, the shock interaction locates at $Z=14.5$ and the associated expansion waves emanating from the shock intersection strike the wing surface near the leading edge, reducing the pressure considerably. The present results reveal that this effect is more significant on the windward surface than on the leeward one. Since the effect of expansion wave is restricted only in a small range along the leading edge, the pressure begins to increase again as Z increases because the local swept angle of the leading edge is still decreasing there, thus resulting in a minimum pressure at $Z=15.2$. The same trend in the leading-edge pressure has been observed in the numerical results proposed by Kutler[4] and Bertin.[19]

In the case of $\alpha=0$ deg, on the other hand, although the physical feature of the shock-wave interaction may be the same qualitatively as that in the case of $\alpha=10$ deg, no local minimum pressure along the leading edge can be observed. Since the shock-wave interaction in this case takes place at $Z=16$, at which the local swept angle of the leading edge becomes nearly minimum, the effect of the associated expansion waves is presumably merged in the subsequent pressure decrease due to the increase in local swept angle. This circumstance will be recognized from the fact that a fairly

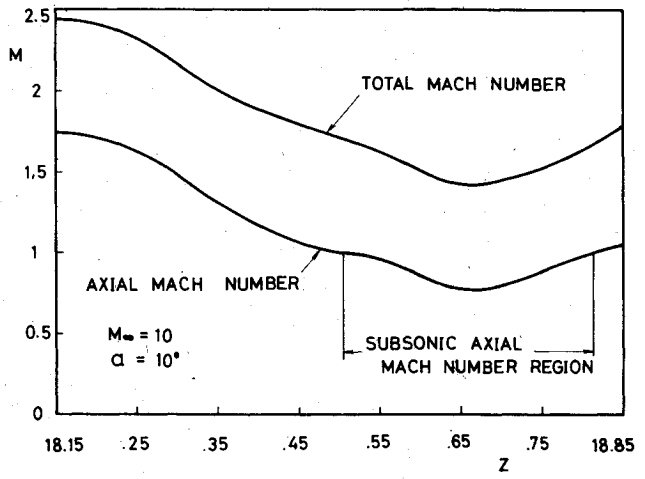

Fig. 11 Longitudinal Mach number distribution.

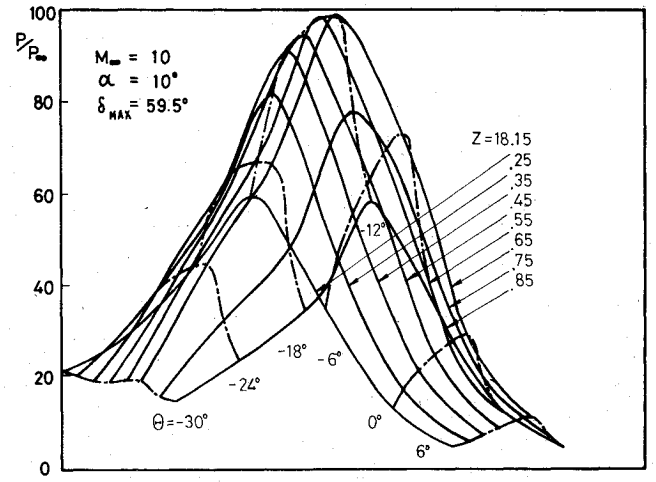

Fig. 12 Surface pressure distribution in the embedded region.

abrupt decrease in leading-edge pressure occurs near downstream of the peak pressure. Also presented in Fig. 7 are the numerical results of pressure in the symmetry plane calculated by Thomas[16] for a 80 deg slab delta wing at a 10 deg angle of attack and Mach 10. Irrespective of the body configurations, the pressure seems to be in good agreement.

Pressure contours on the body surface are shown in Fig. 8. The upper half of the body corresponds to the leeward surface and the lower half to the windward surface. The thick lines in the figure indicate crossflow shock waves. A region of very high pressure occurs near the leading edge, which is magnified on the windward side.

In order to demonstrate the capability of the present method for calculating an embedded region with subsonic Mach numbers in the marching direction, the planform of the wing is modified as illustrated in Fig. 9, where the minimum swept angle of the modified wing leading edge is 30.5 deg at the station $Z=18.65$ and the dashed line indicates the original planform without the subsonic region. These shapes are represented by parabolic curves and the leading edge becomes parallel to the body axis at $Z=19.0$. The region to be solved by the time-dependent method is taken to be $Z=18.15$-18.85. At the former station, the flow quantities are given by that obtained from the marching procedure, whereas the latter station is taken far enough downstream for the flow to be supersonic everywhere in the axial direction. Initial values for the time-dependent procedure are given by the numerical solutions of the wing shape presented by the dashed lines in Fig. 9. In this calculation the grid spacing consists of 7 points in the circumferential direction and 11 points in the radial direction for each $\Delta Z=0.1$ interval.

In Fig. 10 the cross-sectional contours of the body and shock wave at $Z=18.75$ are presented, in which are also indicated the side boundaries bounding the embedded subsonic axial Mach number region. Despite the few mesh points in the radial direction, the embedded shock waves fit fairly well, although a slight distortion of the bow shock wave can be seen near the wing leading edge.

Longitudinal Mach number distribution along the wing leading edge is shown in Fig. 11, which indicates clearly the existence of the region of subsonic axial Mach number, though the total Mach number is supersonic. Surface pressure distribution in the embedded region is given in Fig. 12. The left side of the figure corresponds to the windward side and the right side to the leeward side. The maximum pressure of $P/P_\infty=98$ occurs at $Z=18.65$ and the corresponding value obtainable from Newtonian theory is $P/P_\infty=104$.

Conclusions

An explicit finite-difference scheme based on the floating fitting technique has been developed for three-dimensional supersonic flows involving shock-shock interactions and the numerical results have been presented to demonstrate the capability of the present method to calculate the flowfield about wing/body combinations. Although data for comparison is sparse, some of the present results are confirmed to be valid in the light of the other experimental and numerical results.

It has been shown that the present approach, which consists of an alternate use of the time-dependent and marching procedures, is capable of efficiently calculating the local embedded region where the flow velocity in the marching direction is subsonic. Since this approach is easily adaptable to the conventional marching schemes and is applicable without any difficulty for even the local embedded region with essentially subsonic Mach numbers, it magnifies utility and applicability of the numerical method to complicated three-dimensional flows.

References

[1] Rakich, J. V., Bailey, H. E., and Park, C., "Computation of Nonequilibrium Three-Dimensional Inviscid Flow over Blunt Nosed Bodies Flying at Supersonic Speed," AIAA Paper 75-835, June 1975.

[2] Chu, C. W., "Supersonic Flow about Slab Delta Wings and Wing-Body Configurations," *Journal of Spacecraft and Rockets,* Vol. 10, Nov. 1973, pp. 741-742.

[3] Attorre, L. D., Bilyk, M. A., and Sergeant, R. J., "Three Dimensional Supersonic Flow Field Analysis of the B-1 Airplane by a Finite-Difference Technique," AIAA Paper 74-189, Jan. 1974.

[4] Kutler, P., Reinhardt, W. A., and Warming, R. F., "Multi-Shocked Three Dimensional Supersonic Flowfields with Real Gas Effects," *AIAA Journal,* Vol. 11, May 1973, pp. 657-664.

[5] Solomon, J. M., Ciment, M., Ferguson, R. E., and Bell, J. B., "Inviscid Flowfield Calculations for Re-entry Vehicles with Control Surfaces," *AIAA Journal,* Vol. 15, Dec. 1977, pp. 1742-1749.

[6] Moretti, G., "On the Matter of Shock Fitting," *Proceedings of the Fourth International Conference on Numerical Methods in Fluid Dynamics, Lecture Notes in Physics,* June 1974, pp. 287-292.

[7] Moretti, G., Grossman, B., and Marconi, F., "A Complete Numerical Technique for the Calculation of Three Dimensional Inviscid Supersonic Flows," AIAA Paper 72-192, Jan. 1972.

[8] Marconi, F., Salas, M., and Yaeger, L., "Development of a Computer Code for Calculating the Steady Super/Hypersonic Inviscid Flow around Real Configurations," NASA CR-2675, April 1976.

[9] Moretti, G., "Experiments in Multi-Dimensional Floating Shock Fitting," PIBAL Rept. 73-18, 1973.

[10] Salas, M. D., "Shock Fitting Method for Compressible Two Dimensional Supersonic Flow," *AIAA Journal,* Vol. 14, May 1976, pp. 583-588.

[11] Daywitt, J., Kutler, P., and Anderson, D., "Floating Shock Fitting for Cones at Large Incidence," *AIAA Journal,* Vol. 16, April 1978, pp. 385-392.

[12] Marconi, F. and Moretti, G., "Three Dimensional Supersonic Flows with Subsonic Axial Mach Numbers," AIAA Paper 76-383, July 1976.

[13] Marconi, F. and Koch, F., "An Improved Supersonic Three-Dimensional External Inviscid Flow Field Code," NASA CR-3108, 1979.

[14] Yamamoto, Y. and Karashima, K., "Floating Shock Fitting for Three-Dimensional Inviscid Supersonic Flows, Part I," *Transactions of the Japan Society for Aeronautical and Space Sciences,* Vol. 23, No. 59, May 1980, pp. 1-17.

[15] MacCormack, R. W., "The Effect of Viscosity in Hypervelocity Impact Cratering," AIAA Paper 69-354, 1969.

[16] Thomas, P. D., Vinokur, M., and Bastianon, R. A., "Numerical Solution for Three-Dimensional Inviscid Supersonic Flow," *AIAA Journal,* Vol. 10, July 1972, pp. 887-894.

[17] Kentzer, C. P., "Discretization of Boundary Conditions on Moving Discontinuities," *Proceedings of the Second International Conference on Numerical Methods in Fluid Dynamics, Lecture Notes in Physics,* Vol. 8, 1970, pp. 108-113.

[18] Edney, B., "Anomalous Heat Transfer and Pressure Distributions on Blunt Bodies at Hypersonic Speeds in the Presence of Impinging Shock," Aeronautical Research Institute of Sweden, FFA Rept. 115, 1968.

[19] Bertin, J. J., Graumann, B. W., and Goodrich, W. D., "Analysis of High Velocity and Real Gas Effects on the Shock-Interference Pattern for Delta-Wing Orbiters," AIAA Paper 74-522, 1974.

[20] Hunt, B. L. and Lamount, P. J., "The Confluence of Three Shock Waves in Three Dimensional Flow," *Aeronautical Quarterly,* Vol. 29, Feb. 1978, pp. 18-27.

[21] Barnwell, R. W., "A Time-Dependent Method for Calculating Supersonic Angle of Attack Flow about Axisymmetric Blunt Bodies with Sharp Shoulders and Smooth Nonaxisymmetric Blunt Bodies," NASA TN-D-6283, Aug. 1971.

[22] Lomax, H. and Inoue, M., "Numerical Analysis of Flow Properties about Blunt Bodies Moving at Supersonic Speeds in an Equilibrium Gas," NASA TR-R-204, July 1964.

[23] Betram, M. H. and Everhart, P. E., "An Experimental Study of the Pressure and Heat-Transfer Distribution on a 70° Slab Delta Wing in Hypersonic Flow," NASA TR-R-153, Dec.